Luminescence, Theory

Mohammad A Omary and Howard H Patterson, University of Maine, Orono, ME, USA

This article is reproduced from the previous edition, volume 2, pp 1186–1207, © 1999, Elsevier Ltd.

Introduction

Luminescence refers to the emission of light from an excited electronic state of a molecular species. In the case of photoluminescence, a molecule absorbs light of wavelength λ_1 decays to a lower energy excited electronic state, and then emits light of wavelength λ_2, as it radiatively decays to its ground electronic state. Generally, the wavelength of emission, λ_2, is longer than the excitation wavelength but in resonance emission $\lambda_1 = \lambda_2$. Luminescence bands can be either fluorescence or phosphorescence, depending on the average lifetime of the excited state which is much longer for phosphorescence than fluorescence. The relative broadness of the emission band is related to the relative difference in equilibrium distance in the excited emitting state versus the ground electronic state.

Photoluminescence of a molecular species is different from emission of an atomic species. In the case of atomic emission, both the excitation and the emission occur at the same resonance wavelength. In contrast, excitation of a molecular species usually results in an emission that has a longer wavelength than the excitation wavelength.

If a chemical reaction results in the production of a molecular species in an excited electronic state that emits light, this phenomenon is termed chemiluminescence. Chemiluminescence usually occurs in the gas or liquid phase. In contrast, photoluminescence can occur in the gas, liquid or solid phases.

The next two sections provide a discussion of the basic principles of luminescence spectroscopy, which include the electronic transitions and the important parameters determined from luminescence measurements. Then follow two sections that describe the general characteristics of luminescence measurements and one which provides two case studies for organic and inorganic luminophores. The remainder of the article covers more specific topics and phenomena in luminescence spectroscopy, namely quenching, energy transfer, exciplexes and chemiluminescence. The examples in this article were selected to cover multidisciplinary areas of science.

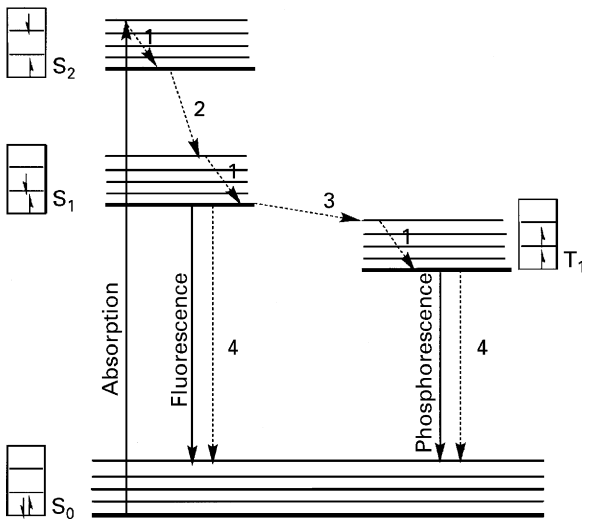

Figure 1 The Jablonski diagram. Radiative and non-radiative processes are depicted as solid and dashed lines, respectively.

Electronic Transitions and Relaxation Processes in Molecular Photoluminescence

The Jablonski Energy Level Diagram

The radiative and non-radiative transitions that lead to the observation of molecular photoluminescence are typically illustrated by an energy level diagram called the Jablonski diagram. Figure 1 shows a Jablonski diagram that explains the mechanism of light emission in most organic and inorganic luminophores. The spin multiplicity of a given electronic state can be either a singlet (paired electrons) or a triplet (unpaired electrons). The ground electronic state is normally a singlet state and is designated as S_0 in Figure 1. Excited electronic states are either singlet (S_1, S_2) or triplet (T_1) states.

When the molecule absorbs light an electron is promoted within $10^{-14}-10^{-15}$ s from the ground electronic state to an excited state that should possess the same spin multiplicity as the ground state. This excludes a triplet excited state as the final state of electronic absorption because the selection rules for electronic transitions dictate that the spin state should be maintained upon excitation. A plethora of non-radiative and radiative processes usually occur following the absorption of light en route to the observation of molecular luminescence. The following is a description of the different types of non-radiative and radiative processes.

Non-Radiative Relaxation Processes

Vibrational Relaxation

Excitation usually occurs to a higher vibrational level of the target excited state (see below). Excited molecules normally relax rapidly to the lowest vibrational level of the excited electronic state. This non-radiative process is called 'vibrational relaxation'. Vibrational relaxation processes occur within 10^{-14}–10^{-12} s, a time much shorter than typical luminescence lifetimes. Therefore, such processes occur prior to luminescence.

Internal Conversion

If the molecule is excited to a higher-energy excited singlet state than S_1 (such as S_2 in Figure 1), a rapid non-radiative relaxation usually occurs to the lowest-energy singlet excited state (S_1). Relaxation processes between electronic states of like spin multiplicity such as S_1 and S_2 are called 'internal conversion'. These processes normally occur on a time scale of 10^{-12} s.

Intersystem Crossing

Non-radiative relaxation processes between different excited states are not limited to states with the same spin multiplicity. A process in which relaxation proceeds between excited states of different spin multiplicity is called 'intersystem crossing'. The relaxation from S_1 to T_1 in Figure 1 is an example of an intersystem crossing.

Intersystem crossing is generally a less probable process than internal conversion because the spin multiplicity is not conserved. Because of the lower probability for intersystem crossing processes they occur more slowly ($\sim 10^{-8}$ s) than internal conversions. Intersystem crossing processes become more important in molecules containing heavy atoms such as iodine and bromine in organic luminophores and metal ions in inorganic luminophores (transition-metal complexes). Significant interaction between the spin angular momentum and the orbital angular momentum (spin–orbit coupling) becomes more important in the presence of heavy atoms and, consequently, a change in spin becomes more favourable. In solution, the presence of paramagnetic species such as molecular oxygen increases the probability of intersystem crossing. In transition metal complexes, intersystem crossing processes become increasingly important as one proceeds from complexes of the 3d-block elements to those of the 4d- and 5d-blocks.

Non-Radiative De-Excitation

The excitation energy stored in the molecules following absorption must be dissipated owing to the law of conservation of energy. The aforementioned non-radiative processes occur very rapidly and only release very small amounts of energy. The rest of the stored energy will be dissipated either radiatively, by emission of photons (luminescence), or non-radiatively, by the release of thermal energy. The non-radiative decay of excitation energy which leads to the decay of the excited molecules to the ground electronic state is called 'non-radiative de-excitation'. These processes result in the release of infinitesimal amounts of heat that cannot normally be measured experimentally. The experimental evidence for non-radiative de-excitation processes is the quenching of luminescence. A major route for non-radiative de-excitation processes is energy transfer to the solvent or non-luminescent solutes in the solution. In the solid state, crystal vibrations (phonons) provide the mechanism for non-radiative de-excitation.

Radiative Processes: Fluorescence and Phosphorescence

The spin selection rule for electronic transitions (both absorption and emission) states that 'spin-allowed' transitions are those in which the spin multiplicity is the same for the initial and final electronic states. Therefore, spin-allowed transitions are more likely to take place than spin-forbidden transitions. 'Fluorescence' refers to the emission of light associated with a radiative transition from an excited electronic state that has the same spin multiplicity as the ground electronic state. Fluorescence is depicted by the radiative transition $S_1 \rightarrow S_0$ in Figure 1. Since fluorescence transitions are spin-allowed, they occur very rapidly and the average lifetimes of the excited states responsible for fluorescence are typically $<10^{-6}$ s.

Electronic transitions between states of different spin multiplicity are 'spin-forbidden' which means that they are less probable than spin-allowed transitions. However, spin-forbidden transitions become more probable when spin–orbit coupling increases. The factors that increase the probability of phosphorescence are the same factors discussed above that increase the probability of intersystem crossing. Therefore, if the triplet excited state is populated by intersystem crossing then luminescence might occur from the triplet state to the ground state. 'Phosphorescence' refers to the emission of light associated with a radiative transition from an excited electronic state that has a different spin multiplicity from that of the ground electronic state. Phosphorescence is depicted by the radiative transition $T_1 \rightarrow S_0$ in Figure 1. Since phosphorescence transitions are spin-forbidden, they occur slowly and the average lifetime of the excited states responsible for phosphorescence typically range from 10^{-6} s to several seconds. Therefore, some textbooks refer to phosphorescence as 'delayed fluorescence'. Photoluminescence refers to both fluorescence and phosphorescence.

Excited-State Distortions and the Franck–Condon Principle

Luminescence spectroscopy can be used to gain information about the geometry of a molecule in an excited

electronic state. Such information provides an understanding of the difference in the bonding properties of an excited state relative to the ground state. These properties can be better understood when the electronic transitions are discussed in the context of the potential surfaces of the ground and excited states.

Electronic absorption of light occurs within 10^{-15} s. Since this time is extremely short, the nuclei are assumed to be 'frozen' during the time scale of absorption. Therefore, the transitions between various electronic levels are depicted as 'vertical' transitions in energy level diagrams. This assumption of negligible nuclear displacement during electronic transitions is known as the 'Franck–Condon principle'. **Figure 2** illustrates the Franck–Condon principle. Electronic excited states usually have different geometries than the ground state and, consequently, different equilibrium distances. Since electronic transitions are vertical, only transition A in **Figure 2** occurs. Transition C involves an excited state that is largely displaced from the ground state and thus no vertical transition is possible to this state. Transition B, on the other hand, terminates in the lowest vibrational level of the excited state. **Figure 2** shows that this transition cannot occur vertically, either. The three transitions depicted in **Figure 2** explain why in the Jablonski diagram (**Figure 1**): (i) the absorption was depicted to a higher vibrational level of the S_2 excited state than the $v = 0$ level, and (ii) no direct excitation to the triplet excited state (T_1) was depicted.

Usually, the nuclei of excited molecules are displaced from their ground state positions. The displacement is caused by differences in the bonding properties between

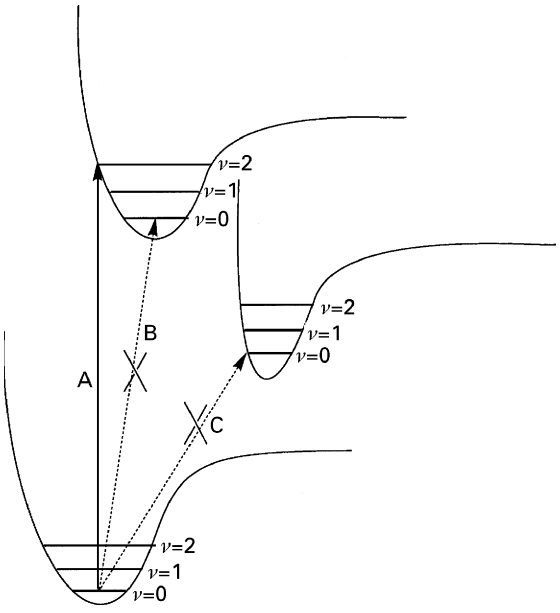

Figure 2 The Franck–Condon principle. Only vertical electronic transitions are allowed.

the molecular orbitals that represent the ground and excited states, respectively. The extent of the nuclear displacement varies from one case to another. **Figure 3** illustrates two cases (a) and (b) of excited state distortion. The transitions depicted in **Figure 3** are called 'vibronic transitions'. A vibronic transition refers to a transition that involves a change in both electronic and vibrational states.

The case shown in **Figure 3(b)** represents an extreme case in which the excited state distortion is virtually zero. As a result, the electronic transition for which $v = 0$ in both the ground and excited states (called the 0–0 vibronic transition) has the greatest probability and, thus, the strongest intensity in both absorption and emission spectra. When excited state distortion is significant, as in **Figure 3a**, the 0–0 transition becomes much less probable and so its intensity becomes much weaker than other 0–v vibronic transitions with higher v values.

The probability (P) of the occurrence of a vibronic transition is proportional to the square of the *Franck–Condon factor*, which is defined as the overlap integral of the vibrational wavefunctions, $\Psi(v)$. Therefore,

$$P \propto |\langle \Psi(v_1)|\Psi(v_2)\rangle|^2 \qquad [1]$$

In many instances the absorption and emission maxima correspond to the same (v_1–v_2) vibrational pair. For example, **Figure 3a** shows that the 0–2 vibronic transition has the strongest intensity in both the absorption and the emission spectra. This is called the 'mirror image' rule and is followed by luminophores whose excited state distortion is zero or small. However, the mirror image rule may not apply for cases where large excited state distortion exists. Examples of each case are provided in the section dealing with organic luminophores.

Quantitative information about excited state distortion can be obtained from the luminescence spectra. For cases where vibronic structure is observed, the excited state distortion can be probed qualitatively simply by identifying the most intense vibronic transition: the larger the value of the vibrational level of the excited state, the larger the excited state distortion (as illustrated in **Figure 3**). Quantitatively, the displacement (Δq) of the excited state equilibrium distance from the corresponding ground state distance can be calculated. The procedure involves the calculation of the Franck–Condon factor as a function of Δq for each vibronic transition. This results in a calculated emission spectrum, which can be compared with the experimental emission spectrum as a function of Δq until a good fit is obtained. The actual Δq would be the value that gives the best fit.

The emission (and absorption) spectra in many practical cases do not show resolved vibronic peaks. This is especially the case in solutions of the luminophores at ambient temperatures. The interaction of excited molecules of the luminophore with solvent molecules (especially polar

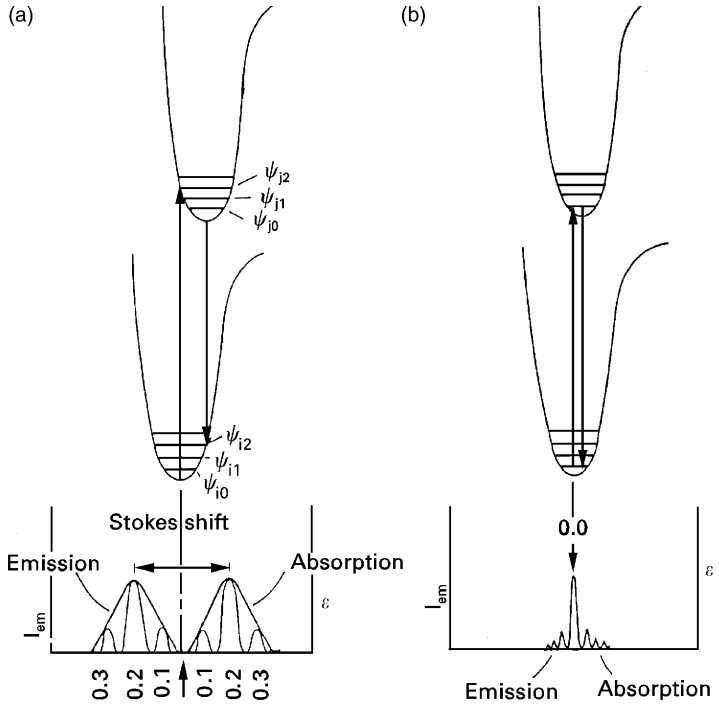

Figure 3 Potential energy diagrams for two cases of excited state distortions: (a) non-zero distortion and (b) zero distortion. The corresponding absorption and emission spectra are shown below. Reproduced with permission from Adamson AW and Fleischauer PD (1975) *Concepts of Inorganic Photochemistry*, p. 4. New York: Wiley-Interscience.

solvents) is responsible for this broadening. There are methods to quantify Δq in these cases with the aid of some computer programs, but the description of these methods is beyond the scope of this article. In the section on inorganic exciplexes, nevertheless, we provide an example in which Δq is evaluated theoretically for a system that exhibits structureless emission bands.

Another quantitative measure of excited state distortion is the *Stokes shift*, defined as the energy difference between the emission and absorption peak maxima for the same electronic transition. The lower part of **Figure 3a** illustrates how the Stokes shift is evaluated in typical cases. The Stokes shift of the rare case shown in **Figure 3b** is zero because the absorption and emission spectra have the same peak positions. The band width can also be used to quantify excited state distortions. The band width is normally quantified in terms of the full-width-at-half-maximum (fwhm). The value of fwhm is calculated as the energy difference between the band positions that have intensities equal to one half the peak maximum, assuming a gaussian shape is obtained for the emission band. In the absence of excited state distortions the emission bands appear as sharp peaks with very small fwhm values (**Figure 3b**), whereas in more common cases the electronic bands are much broader because of excited state distortions (**Figure 3a**). In those cases where the emission spectra are devoid of vibronic structure, the fwhm values are calculated for the whole broad band. The Stokes shift and fwhm are parameters for excited state distortion because their values are larger for 0–v vibronic transitions with higher v values. The Stokes shift and fwhm are especially useful in cases where the emission spectra are structureless, because of the difficulty of carrying out the Δq calculation in such cases.

Emission and Excitation Spectra

In luminescence spectroscopy the emission of the luminophore is monitored. There are two different types of luminescence spectra that can be recorded with modern spectrofluorometers, emission and excitation spectra. Note that although the name implies that these instruments measure only fluorescence, spectrofluorometers can also measure phosphorescence, especially when special accessories are added. Spectrofluorometers contain both an excitation monochromator and an emission monochromator. In emission spectra, the excitation wavelength is fixed and the emission monochromator is scanned. The excitation is usually fixed at a wavelength at which the sample has significant absorbance. In excitation spectra, on the other hand, the emission wavelength is fixed and the excitation monochromator is scanned. The emission is normally fixed at a wavelength that corresponds to the emission peak of the sample.

Theoretically, the excitation spectra should mimic the absorption spectra of the luminophores. However, the

lamp output is wavelength-dependent. For example, a common light source in modern spectrofluorometers is a xenon lamp. The output of this lamp is a continuum in the range ~200–1200 nm. The radiation curve approximates blackbody radiation with a maximum near 550 nm and a sharp decline at short wavelengths. A correction is, therefore, needed for the lamp background in order for the excitation spectra to correlate with the absorption spectra. Corrected excitation spectra are usually obtained by using a *quantum counter*, a strong luminophore capable of absorbing virtually all incident light over a wide range of wavelength. Rhodamine B is a commonly used quantum counter. Concentrated solutions of rhodamine B absorb virtually all the incident light in the 220–600 nm range. The excitation spectrum of rhodamine B monitoring its emission maximum (633 nm) is determined only by the lamp output in the 220–600 nm range (**Figure 4a**).

Corrected excitation spectra of luminophores are obtained by dividing the uncorrected spectra by the excitation spectrum of the quantum counter. A common improvement in the corrected excitation spectra versus the uncorrected spectra is to eliminate the sharp 'spikes' of the xenon lamp between 450 and 500 nm (**Figure 4(a)**). This makes the excitation spectra of many luminophores very similar to their absorption spectra. However, more dramatic differences may exist, especially for luminophores which absorb in the UV region. An example of such a luminophore is the silver complex $[Ag(CN)_2^-]$. **Figure 4b** shows the corrected and uncorrected excitation spectra of $[Ag(CN)_2^-]$ doped in NaCl crystals. Note that the corrected excitation spectra are significantly different from the uncorrected spectra. This difference is attributed to the low output of the xenon lamp at wavelengths shorter than 280 nm (**Figure 4a**), at which $[Ag(CN)_2^-]$ species absorb strongly.

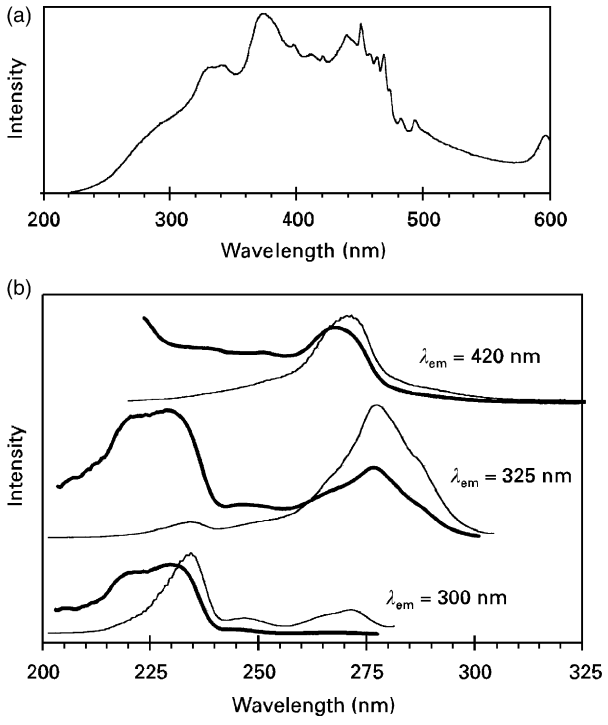

Figure 4 Correction of the excitation spectra by the quantum counter method: (a) excitation spectrum of rhodamine B; (b) excitation spectra of $[Ag(CN)_2^-]$/NaCl doped crystals monitoring the emission at different wavelengths. Corrected and uncorrected spectra are shown as thick and thin lines, respectively.

Absorption and excitation spectra are complementary. The necessity to obtain a correction for the excitation spectra represents a disadvantage. There are advantages, however, for excitation spectra over absorption spectra. The much higher sensitivity of luminescence techniques compared to absorption techniques is an obvious advantage for excitation spectra. The greater sensitivity of luminescence techniques stems from the fact that the luminescence intensity can be enhanced by increasing the intensity of the excitation source, which is not the case in absorption. The greater sensitivity of luminescence techniques is, however, accompanied by less precision compared to absorption techniques. The relative ease of acquiring excitation spectra for some materials such as solids represents another advantage over absorption measurements. Finally, excitation spectra can provide valuable information about excited state processes such as energy transfer (see below) that cannot be obtained by absorption spectra.

Luminescence Lifetimes

Theory

Consider the simplest case in which a molecule A absorbs light and is in an excited electronic state denoted by $^*A$. If the molecule has a single pathway for decay, say fluorescence, we can write the following equation:

$$^*A \rightarrow A + h\nu \qquad [2]$$

This is a first-order process whose rate can be expressed mathematically as:

$$-d[^*A]/dt = k_f[^*A] \qquad [3]$$

where k_f is the rate constant of the fluorescence decay (eqn [2]). The reciprocal of k_f is called the fluorescence lifetime τ_f ($\tau_f = 1/k_f$). Integration of eqn [3] gives:

$$[^*A] = [^*A]_o \exp(-t/\tau_f) \qquad [4]$$

Hence, a plot of ln $[^*A]$ versus time (t) should give a straight line with a slope of $1/\tau_f$. The value of $[^*A]$ is determined from the fluorescence intensity. Experimentally, lifetime measurements are obtained using a pulsed laser source. Pulsing leads to the population of the excited state of A, followed by emission of light by $^*A$ with a time profile

according to eqn [4]. Figure 5 shows a schematic description of a luminescence decay curve (a) and the plot used for the determination of the excited state lifetime (b).

Next, consider the case where $^*A$ can exhibit fluorescence (eqn [2]) and also non-radiative decay:

$$^*A \rightarrow A + \text{vibrational energy} \quad [5]$$

with a rate constant of k_{nr}. The decay of $^*A$ can now be described as:

$$-d[^*A]/dt = k_f[^*A] + k_{nr}[^*A] = (k_f + k_{nr})[^*A] \quad [6]$$

In this case the lifetime τ becomes:

$$\tau = 1/(k_f + k_{nr}) \quad [7]$$

or the reciprocal of the sum of k_f and k_{nr}.

Generally, the non-radiative rate constant decreases at lower temperatures. As the temperature (T) approaches absolute zero, τ approaches $1/k_f$. A plot of $1/\tau$ versus T extrapolated to $T = 0$ K allows one to determine k_f as the value of the intercept (see the example in the case study on inorganic luminophores). Therefore, the value of the fluorescence lifetime (τ_f) is determined as $1/k_f$. Note that the treatment described in this section applies for both fluorescence and phosphorescence lifetimes and not just for fluorescence.

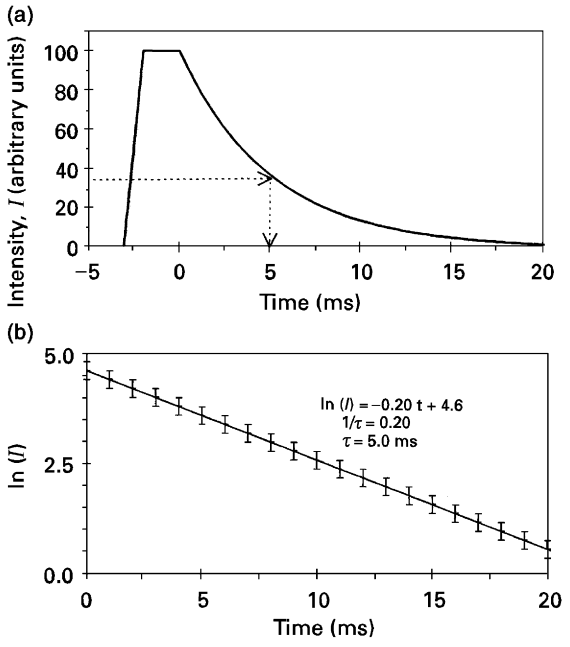

Figure 5 Experimental determination of excited state lifetimes: (a) a plot of the intensity (I) versus time after the laser pulse. The lifetime corresponds to the time at which the intensity decays to 1/e of its maximum value; (b) a plot of ln (I) versus time after laser pulse. The lifetime here can be calculated directly from the slope of the linear equation.

Now consider a final lifetime case in which two states are thermally populated at a temperature T. If excited state 1 has a lifetime τ_1 and excited state 2 has a lifetime τ_2, the observed lifetime τ_{obs} will be a weighted average of the two lifetimes:

$$\tau_{obs} = (n_1/N)\tau_1 + (n_2/N)\tau_2 \quad [8]$$

with $N = n_1 + n_2$. Assuming that excited states 1 and 2 are non-degenerate and using the Boltzmann distribution function gives:

$$\tau_{obs} = \{[\tau_1 + \tau_2 \exp(-\Delta E/kT)]/[1 + \exp(-\Delta E/kT)]\} \quad [9]$$

where ΔE is the energy difference between states 1 and 2 and k is the Boltzmann constant. Fitting τ_{obs} versus T to eqn [9] allows the determination of the value of ΔE as well as τ_1 and τ_2.

Fluorescence versus Phosphorescence Lifetimes

A major advantage of luminescence lifetime measurements is their use for spectral assignment. Specifically, the assignment of the luminescence bands as fluorescence or phosphorescence is primarily determined via luminescence lifetime measurements. As a rule of thumb, lifetimes on the order of micro-seconds and longer (milliseconds, seconds) are normally indicative of phosphorescence, while fluorescence lifetimes are normally on the sub-microsecond level (nanoseconds, picoseconds etc). It should be noted, however, that fluorescence and phosphorescence lifetime values vary from one case to another, depending on the system under study as well as other factors such as the extent of excited state distortion. This causes some subjectivity in the assignment, especially when the measured lifetimes are at borderline levels between the aforementioned levels of fluorescence and phosphorescence lifetimes. The clearest cases are those in which fluorescence and phosphorescence bands are both present in one system. In these cases, the phosphorescence bands exhibit lifetimes that are orders of magnitude longer than the lifetimes of the corresponding fluorescence bands. An example is given for such a case in the section on inorganic luminophores.

Luminescence Quantum Yields

The quantum yield is a luminescence property that is related to lifetimes. The luminescence quantum yield (Φ) is the ratio of the number of photons emitted to the number of photons absorbed. Therefore, the maximum value of Φ is 1. In practice, the quantum yield is less than unity for virtually all luminescent materials. The reason is the large number of non-radiative processes that lead to a decrease in the number of emitted photons. The

quantum yield can be defined in terms of the rate constants of the radiative (k_{rad}) and non-radiative (k_{nr}) processes according to eqn [10]:

$$\Phi = \frac{\sum k_{rad}}{\sum k_{rad} + \sum k_{nr}} \quad [10]$$

The k_{rad} term includes the rate of fluorescence and phosphorescence while the k_{nr} term includes the rate constants of all the non-radiative processes described previously. Remembering that $\tau_f = 1/k_f$ and also using eqn [7], one can express the quantum yield of the fluorescence (Φ_f) in terms of the luminescence lifetimes as:

$$\Phi_f = \frac{k_f}{k_f + \sum k_{nr}} = \frac{\tau}{\tau_f} \quad [11]$$

A variety of factors are believed to influence the luminescence quantum yields of luminophores.

The Transition Type

Because luminescence is a technique of electronic spectroscopy, the same selection rules apply for luminescence as those that apply for absorption. For organic compounds, the most common luminescence bands are due to π^*–π and π^*–n transitions. The σ^*–σ transitions, although strongly allowed, are not normally seen because of their high energies in most organic compounds. The spin selection rules also apply. Consequently, fluorescence in most luminescent organic compounds is much stronger than phosphorescence (see the example in the section on organic luminophores). For inorganic compounds, the luminescence transitions may involve the energy levels of the ligands (intra-ligand transitions), the metal ions (d–d transitions), or both the metal and the ligand (charge transfer transitions). Intra-ligand transitions are similar to the transitions discussed above for organic compounds. The d–d transitions are usually forbidden transitions, so the corresponding absorption and emission bands are generally weak. Charge transfer transitions are strongly allowed and can occur either from the ligand orbitals to the metal orbitals (ligand-to-metal charge transfer, LMCT) or vice versa (metal-to-ligand charge transfer, MLCT).

Structural Rigidity

Molecules that have *rigid* structures normally exhibit strong luminescence. Three examples are shown in Scheme 1. In each pair the fluorophore on the left has the more rigid structure, resulting in greater luminescence quantum yield. Note in the third example that the stronger luminescence intensity is due to the complexation with a metal ion (i.e. the complex is more rigid than the free ligand). The higher luminescence quantum yields for *rigid* luminophores are probably due to the inhibition of the internal conversion rates and vibrational motion in these compounds.

Substitution

The nature of the substituents on, say, an aromatic ring may increase or decrease the quantum yield. For example, halogen and ketone substituents on anthracene generally decrease the fluorescence quantum yield. In contrast, the quantum yield of diphenyl anthracene is nearly unity (compared with $\Phi_f = 0.4$ for unsubstituted anthracene). Phosphorescence becomes an important factor if the substituents contain heavy atoms (for example halogens). In this case the reduction in fluorescence is accompanied by an increase in phosphorescence. This effect (called the *heavy atom effect*) is specially important in inorganic luminophores because of the involvement of the metal ions. The strong spin–orbit coupling in metal ions leads to the relaxation of the spin selection rules. Therefore, most inorganic luminophores exhibit strong phosphorescence (see below).

Other Factors

Many other factors affect luminescence quantum yields. Among these factors are temperature, solvent, phase and pH. A reduction in temperature suppresses non-radiative processes and thus increases Φ. This is why it is common to run luminescence experiments at cryogenic temperatures. The solvent is involved in many non-radiative processes. An increase in the viscosity of the solvent generally decreases the rate of non-radiative de-excitation. Also, the stretching frequency of the bonds of the

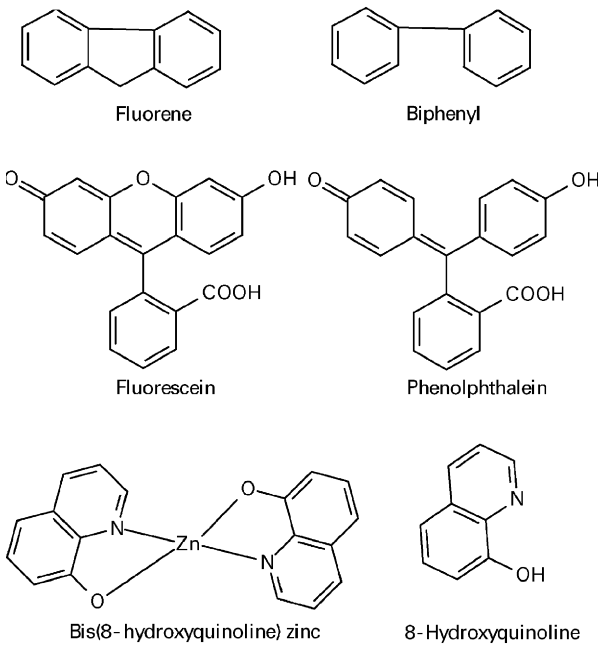

Scheme 1

solvent molecules is an important factor. For example, one of the common procedures to increase the quantum yield is to run the luminescence measurements in deuterated solvents (e.g. D_2O instead of H_2O). The quenching caused by the solvent may be removed by running the luminescence measurements in the solid state instead of solutions (examples are given later). Finally, a change in pH may strongly alter the Φ value because the structure of many luminophores may be different in acidic and basic media.

Case Studies for Photoluminescence

Organic Luminophores

The luminescence properties of anthracene and its derivatives provide an excellent illustration of the relation between the excited state distortion and the profile of the luminescence spectra. Figure 6 shows the luminescence and absorption spectra of anthracene. Note that the extinction coefficient for the singlet–singlet transition is 8 orders of magnitude higher than the value for the singlet–triplet transition. This observation suggests that the absorption and emission bands in the region with $\lambda < 500\,\text{nm}$ are due to a spin-allowed transition (singlet $\leftrightarrow$ singlet), hence the emission in this region is due to fluorescence. On the other hand, the bands in the region with $\lambda > 500\,\text{nm}$ are due to a spin-forbidden transition (singlet $\leftrightarrow$ triplet), hence the emission in this region is due to phosphorescence.

Figure 6 shows that the mirror image rule applies very well to the absorption and fluorescence bands of the $S_0 \leftrightarrow S_1$ transition. Note that among the vibronic bands, the 0–0 and 0–1 transitions have the strongest intensities. These observations suggest that the excited state distortion is very small in anthracene. Figure 6 also shows that there is correlation even between the absorption and phosphorescence characteristic of the $S_0 \leftrightarrow T_1$ transition. However, the mirror image rule does not apply as strongly as it does for the $S_0 \leftrightarrow S_1$ transition. For

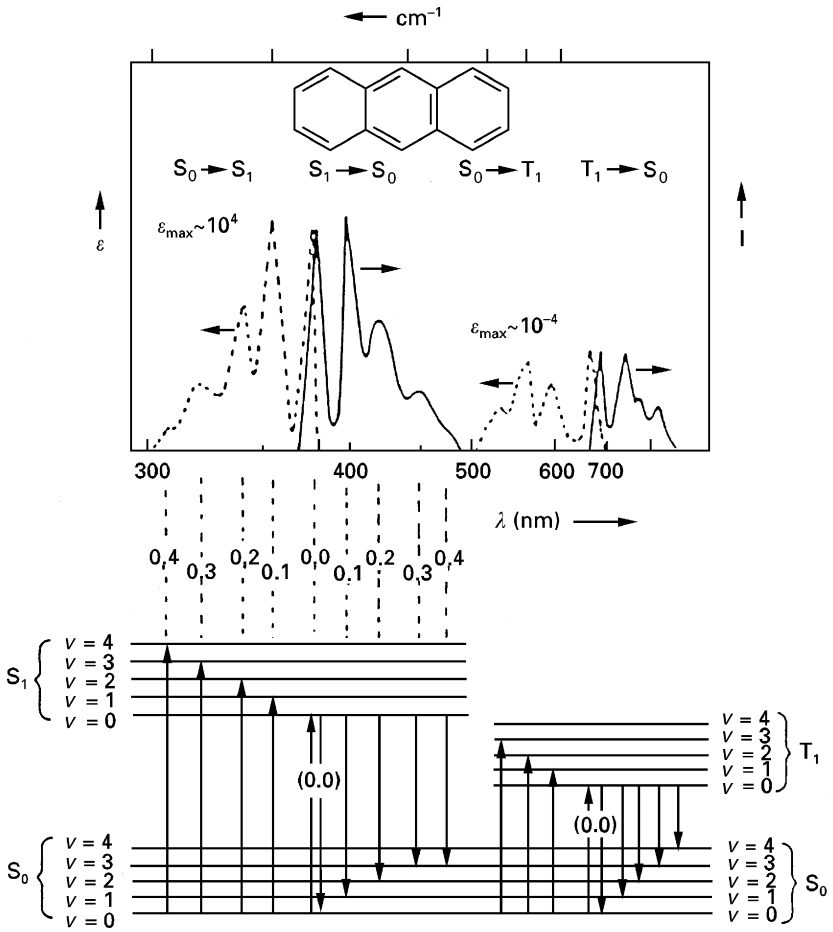

Figure 6 Emission (solid line) and absorption (dashed line) spectra of anthracene in solution. The assignments of the vibronic transitions are shown in the bottom portion of the figure. Reproduced with permission from Turro NJ (1978) *Modern Molecular Photochemistry*, p. 94. Menlo Park: Benjamin/Cummings.

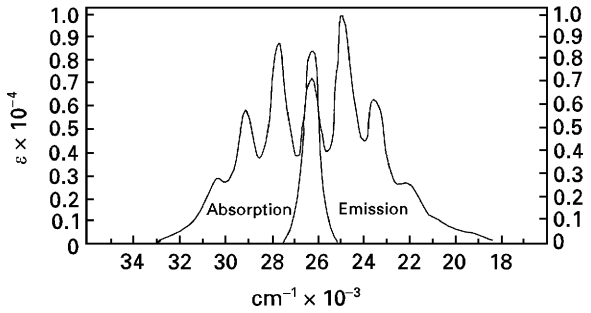

Figure 7 Emission (right) and absorption (left) spectra of 9-anthramide in tetrahydrofuran. Reproduced with permission from Shon RS-L, Cowan DO, and Schmiegel WW (1975) Photodimerization of 9-anthroate esters and 9-anthramide. *The Journal of Physical Chemistry* 79: 2087–2092.

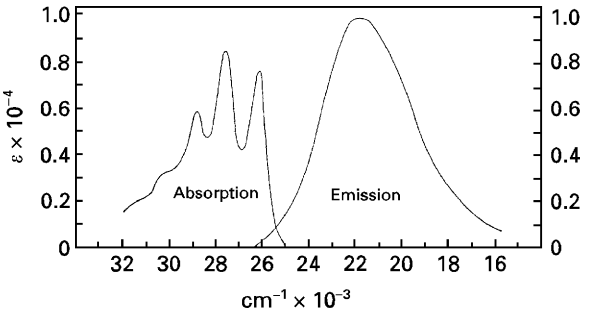

Figure 8 Emission (right) and absorption (left) spectra of cyclohexyl-9-anthroate in benzene. Reproduced with permission from Shon RS-L, Cowan DO, and Schmiegel WW (1975) Photodimerization of 9-anthroate esters and 9-anthramide. *The Journal of Physical Chemistry* 79: 2087–2092.

example, the intensity is greater for the 0–1 transition than for the 0–2 transition in the phosphorescence band, but the opposite trend is seen in the corresponding absorption band. Moreover, while the absorption and emission peaks are nearly superimposed for the 0–0 vibronic peak of the $S_0 \leftrightarrow S_1$ transition, there is a greater separation between the corresponding peaks characteristic of the $S_0 \leftrightarrow T_1$ transition. These observations are consistent with the excited state distortion for the triplet excited state (T_1) being greater than the distortion of the singlet excited state (S_1).

Substitution of hydrogen atoms of anthracene may lead to a geometry change in the excited state. The extent of this change can be probed by luminescence spectroscopy. **Figures 7 and 8** provide an illustration. In **Figure 7**, the absorption and fluorescence spectra are shown for 9-anthramide. Similar geometries of the ground state and the fluorescent excited state of 9-anthramide are illustrated by (i) the applicability of the mirror image rule, (ii) the peaks characteristic of the 0–0 and 0–1 transitions both being strong, and (iii) the absorption and emission peaks being superimposed for the 0–0 transition. The situation is not the same when the substituent on anthracene is changed from an amide group to an ester group. **Figure 8** shows the absorption and emission spectra of cyclohexyl-9-anthroate. Note that the emission spectrum of cyclohexyl-9-anthroate is structureless and the mirror image rule is lost. Also note the large values of the Stokes shift ($\sim 6000\,\mathrm{cm}^{-1}$) and fwhm ($\sim 5000\,\mathrm{cm}^{-1}$). These observations suggest a largely displaced excited state for cyclohexyl-9-anthroate from the ground state geometry of the molecule. In conclusion, **Figures 7 and 8** show that the luminescent excited state is much more distorted for the ester derivative of anthracene (cyclohexyl-9-anthroate) than for the amide derivative of the same molecule (9-anthramide). One can therefore predict that the ester has a greater tendency to undergo photochemical reactions than the amide.

Inorganic Luminophores

The compound $BaPd(CN)_4 \cdot 4H_2O$ provides an excellent example for the differentiation between fluorescence and phosphorescence based on lifetimes and other luminescence properties. Inorganic compounds that exhibit chain structures show interesting luminescence properties in the solid state. The X-ray structure of $BaPd(CN)_4 \cdot 4H_2O$ consists of $[Pd(CN)_4]^{2-}$ square-planar ions stacked in one-dimensional chains with an intrachain Pd–Pd distance of 3.37 Å at room temperature. **Figure 9** shows the luminescence spectrum of $BaPd(CN)_4 \cdot 4H_2O$ at 7 K using a nitrogen pulsed laser for excitation. Two emission bands are observed at $\sim 19 \times 10^3$ and $26 \times 10^3\,\mathrm{cm}^{-1}$ ($\sim$512 and 382 nm, respectively). These bands are designated the *lower energy* (LE) and the *higher energy* (HE) bands, respectively. In **Figure 10** the lifetime of the LE band is plotted versus temperature. A linear fit is obtained. From the resulting equation, the lifetime at 0 K is estimated to be $\sim$2.5 ms and decreases by approximately a factor of 2 for each 30 K temperature rise. The shorter lifetimes at higher temperatures are due to the larger values of k_{nr} at higher temperatures (eqn [7]). In contrast, the HE band has a lifetime shorter than the instrumental resolution of 10 ns. Thus, the lifetime data suggest that the HE band is fluorescence while the LE band is phosphorescence.

Polarized light can be used to study the luminescence bands for $BaPd(CN)_4 \cdot 4H_2O$. The HE band has polarized emission with the phase of polarization of the fluorescence perpendicular to the $Pd(CN)_4^{2-}$ square planar plane (z-direction). In contrast, the LE band has polarized emission with the phase of the polarized light the same as the $Pd(CN)_4^{2-}$ molecular plane (xy-direction). The metal ions in one-dimensional chained compounds are oriented along one particular direction in crystals of layered compounds (along the xy-direction in $BaPd(CN)_4 \cdot 4H_2O$). The absorption band of $BaPd(CN)_4 \cdot 4H_2O$ solid is polarized along the xy-direction. The fact that the HE emission band has the same polarization as the absorption

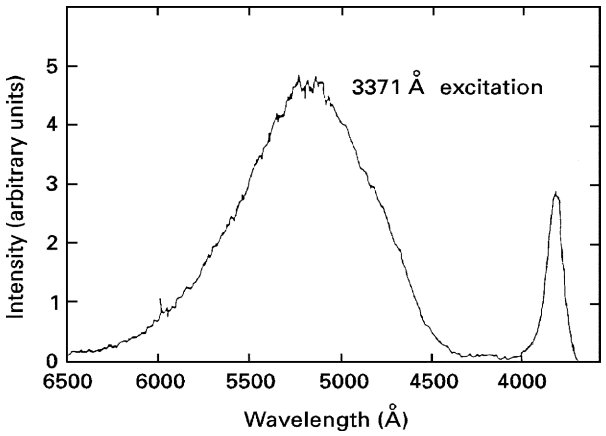

Figure 9 Luminescence spectrum of $BaPd(CN)_4 \cdot 4H_2O$ at 7 K. A nitrogen laser was used for excitation. Reproduced with permission from (Ellenson WD, Viswanath AK, and Patterson HH (1981) Laser-excited luminescence study of the chain compound $BaPd(CN)_4 \cdot 4H_2O$. *Inorganic Chemistry* 20: 780–783).

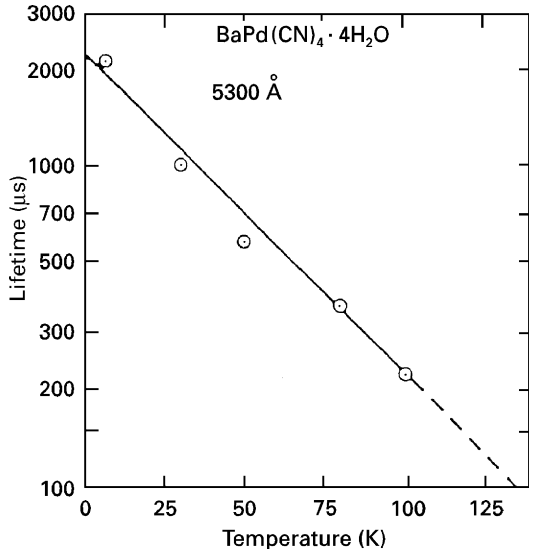

Figure 10 Lifetime of the $19 \times 10^3\,cm^{-1}$ luminescence band of $BaPd(CN)_4 \cdot 4H_2O$ versus temperature. The dashed line is extrapolation to higher temperatures. Reproduced with permission from Ellenson WD, Viswanath AK, and Patterson HH (1981) Laser-excited luminescence study of the chain compound $BaPd(CN)_4 \cdot 4H_2O$. *Inorganic Chemistry* 20: 780–783.

band provides further evidence that the HE band is fluorescence. This is because fluorescence takes place immediately after absorption ($\tau < 10\,ns$) and from the same singlet excited electronic state as the one which absorption populates. In contrast, the LE band occurs from a triplet excited state long after absorption ($\tau = 2.5\,ms$). Because the absorption and the LE emission bands have different excited states, these bands have different polarization. In accordance with the polarization of the HE band along the same direction as the Pd chains, the emission maximum of the HE band undergoes a progressive red shift (longer wavelength, lower energy) as the temperature is decreased. The red shift occurs because cooling leads to a thermal contraction of the intra-chain Pd–Pd distance, which results in a smaller HOMO–LUMO energy gap (HOMO = highest occupied molecular orbital, LUMO = lowest unoccupied molecular orbital). In contrast, the position of the LE band is independent of temperature because this band is not polarized along the Pd chains.

The preceding results can be compared with the selection rules for all the possible electronic transitions obtained from group theory, to give electronic assignments (term symbols) for each of the luminescence bands. The resulting electronic assignments are $^1A_{2u}$ and $^3A_{2u}$ for the HE and LE bands, respectively. A discussion of the concepts of group theory that lead to this assignment is beyond the scope of this article. However, it is enough to note that the term symbols of the HE and LE bands of $BaPd(CN)_4 \cdot 4H_2O$ differ only in the spin multiplicity (superscripts indicate singlet and triplet, respectively). With this in mind, the difference in the excited state distortion between the HE and LE bands can be used to provide further evidence for the band assignment. The lowest energy absorption band of $BaPd(CN)_4 \cdot 4H_2O$ solid has an energy of $\sim 31 \times 10^3\,cm^{-1}$. This gives a Stokes shift of ~ 5000 and $11\,500\,cm^{-1}$ for the HE and LE bands, respectively. Figure 9 shows that the LE band is much broader than the HE band. The fwhm values of the HE and LE bands are 900 and $3300\,cm^{-1}$, respectively. The higher values of the Stokes shift and fwhm for the LE band are consistent with the assignment that the LE band is phosphorescence while the HE band is fluorescence of the same electronic transition. This is the case because the excited state distortion of phosphorescence is greater than that of the fluorescence of the same electronic transition (with a different spin state). The Jablonski diagram shown in Figure 1 illustrates the higher Stokes shift for phosphorescence compared with fluorescence.

In summary, the HE and LE luminescence bands of $BaPd(CN)_4 \cdot 4H_2O$ are assigned as fluorescence and phosphorescence, respectively. The basis of this assignment is the difference between the two bands in the lifetime values, polarization character, temperature dependence, and excited state distortion (Stokes shift and fwhm values).

Finally, an interesting aspect of the luminescence spectrum of $BaPd(CN)_4 \cdot 4H_2O$ is the strong phosphorescence intensity (compared with the relative phosphorescence/fluorescence intensity of anthracene). This is a direct consequence of the strong spin–orbit coupling of palladium. This provides an illustration of the heavy atom effect which is generally more important in inorganic luminophores relative to their organic counterparts.

Quenching of Emission

Theory

In luminescence spectroscopy, quenching refers to any process that leads to a reduction in the luminescence intensity of the luminophore. Static and dynamic quenching are the most common types of luminescence quenching and will be described in the following sections. A third type of quenching also exists, namely 'inner-filter quenching'. An inner-filter effect occurs when the total absorbance of the solution is high (greater than 0.1 au). This leads to a reduction in the intensity of the excitation radiation over the path length. Quenching of this type is not generally categorized among the major quenching process because it is a trivial type of quenching that is not really involved in the radiative and non-radiative transitions in luminescence spectroscopy.

Both static and dynamic quenching require contact of the luminophore with a quencher molecule. This requirement is the basis of the many applications of luminescence quenching. Because there are so many molecules that can act as luminescence quenchers, an appropriate quencher can be selected for any luminophore under study in order to investigate specific properties of the luminophore. An example of biochemical applications of luminescence quenching is given later in this section.

Static Quenching

Static quenching occurs upon the complexation of the luminophore (L) with a quencher (Q):

$$L + Q \rightleftharpoons L - Q \qquad [12]$$

The total concentration of the luminophore, $[L]_0$, is given by:

$$[L]_0 = [L] + [L - Q] \qquad [13]$$

The dependence of the luminescence intensity on the quencher concentration can be derived by considering the association constant for the formation of the L–Q complex, K_s:

$$K_s = \frac{[L - Q]}{[L][Q]} = \frac{[L]_0 - [L]}{[L][Q]} \qquad [14]$$

Rearrangement gives:

$$\frac{[L]_0}{[L]} = 1 + K_s[Q] \qquad [15]$$

Static quenching occurs because the resulting ground state complex is not luminescent and, therefore, the concentration of free L decreases upon its complexation. The ratio $[L]_0/[L]$ is a measure of the decrease of the luminescence intensity due to static quenching. In the absence of the quencher (Q), the luminescence intensity, I_0, is highest because $[L]_0 = [L]$. In the presence of Q, the luminescence intensity, I, decreases due to static quenching. Therefore, the ratio $[L]_0/[L]$ is the same as I_0/I. Substituting in eqn [15] gives the Stern–Volmer equation:

$$I_0/I = 1 + K_s[Q] \qquad [16]$$

A Stern–Volmer plot of I_0/I against [Q] should give a straight line with a slope equal to K_s, which is also known as the Stern–Volmer constant for static quenching.

Dynamic Quenching (Collisional Quenching)

Dynamic or collisional quenching occurs when the lifetime of the fluorophore is reduced, thus reducing the luminescence quantum yield. The mechanism of this type of quenching involves a collision of the excited luminophore molecule ($^*L$) with a quencher molecule (Q). As a result, $^*L$ returns to its ground state without emitting photons and the excitation energy is transferred to Q. The transfer of the excitation energy to Q leads to a reduction of the excited state lifetime of $^*L$ and, therefore, a reduction of the luminescence intensity. It can be shown that the reduction of the luminescence intensity due to dynamic quenching is the same as the corresponding reduction of the excited state lifetime:

$$I_0/I = \tau_0/\tau \qquad [17]$$

where τ_0 and τ refer to the lifetimes in the absence and presence of the quencher, respectively. The Stern–Volmer equation that governs dynamic quenching can be derived on the basis of the kinetic model shown in Figure 11.

The radiative decay rate (k_{rad}) is the reciprocal of the excited state lifetime in the absence of the quencher ($1/\tau_0$). The rates of depopulation of $^*L$ in the absence and presence of Q are given in eqns [18] and [19],

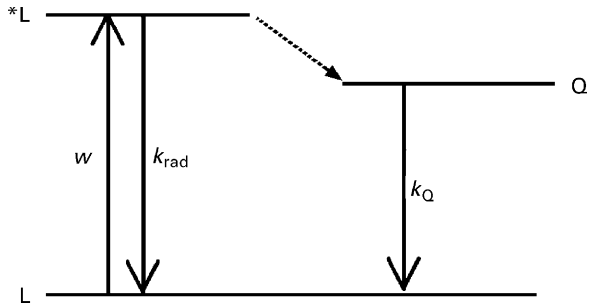

Figure 11 Kinetic model for dynamic quenching. In the notation used w, k_{rad} and k_Q refer to the absorption rate, radiative rate and quenching rate, respectively.

respectively:

$$d[^*L]/dt = w - k_{rad}[^*L]_0 = 0 \quad [18]$$

$$d[^*L]/dt = w - k_{rad}[^*L] - k_Q[^*L][Q] = 0 \quad [19]$$

Substituting $(1/\tau_0)$ for K_{rad}, after rearrangement, gives eqn [20], which is the Stern–Volmer equation for dynamic quenching:

$$I_0/I = 1 + K_Q\,\tau_0[Q] \quad [20]$$

The term $(k_Q\,\tau_0)$ is the Stern–Volmer quenching constant for dynamic quenching, K_D. Therefore, the Stern–Volmer equation for dynamic quenching can be re-written as:

$$I_0/I = 1 + K_D[Q] \quad [21]$$

Note that eqns [16] and [21] are identical in form, and from both equations Stern–Volmer plots can be made in order to obtain the constants K_S and K_D, respectively. This can be carried out simply by measurements of the luminescence intensity in the presence and absence of the quencher. However, such a study does not distinguish between the two mechanisms. The easiest and most definitive way to determine the quenching mechanism is to carry out a study of the lifetimes in the presence and absence of the quencher. The excited state lifetime decreases in the presence of quencher if dynamic quenching is the mechanism involved. Note that according to eqn [17], a Stern–Volmer plot can be obtained by plotting (τ_0/τ) on the y-axis instead of I_0/I:

$$\tau_0/\tau = 1 + K_D[Q] \quad [22]$$

In contrast, the excited state lifetime is invariant in the presence of the quencher if static quenching is the mechanism involved. Therefore, plotting (τ_0/τ) versus [Q] will simply yield a horizontal line parallel to the x-axis ($y = 1$).

Example

Tryptophan residues in a protein luminesce strongly whether they are on the surface of the protein or in its interior. When a quenching experiment is carried out with ionic quenchers, such as the iodide ion, the resulting quenching involves only surface-localized tryptophan residues. On the other hand, non-ionic quenchers, such as acrylamide, are able to penetrate into the interior of the protein and provide quenching constants that are really average constants and give information about both surface and interior tryptophan residues.

One way of separating the fluorescence quenching parameters associated with external and internal fluorophores is to use a double-quenching method in which two quenchers are applied simultaneously. The first quencher is used to selectively quench the fluorescence emission of exposed fluorophores. On the other hand, the second quencher is used to quench the fluorescence emission of both surface and interior fluorophores non-selectively.

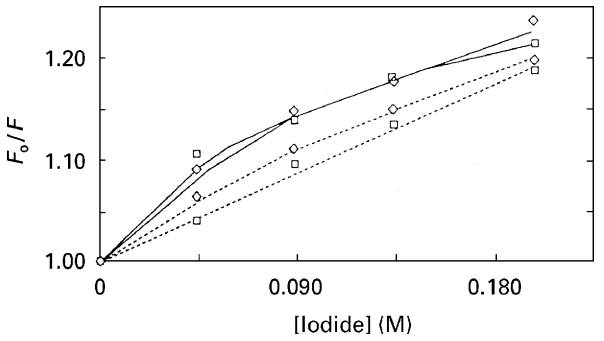

Figure 12 A Stern–Volmer plot for the fluorescence quenching of HDL_1 (solid lines) and HDL_2 (dashed lines). The different legends refer to samples obtained from rats fed with manganese-adequate (◇) and manganese-deficient (□) diet. The fluorescence was monitored at 338 nm (λ_{exc} = 295 nm) characteristic of tryptophan residues. Reproduced with permission from Taylor PN, Patterson HH, and Klimis-Tavatzis DJ (1997) A fluorescence double-quenching study of native lipoproteins in an animal model of manganese deficiency. *Biological Trace Element Research* 60: 69–80.

Figure 12 shows Stern–Volmer plots of two samples of high density lipoproteins, HDL_1 and HDL_2 (referring to different densities of high density lipoproteins). These samples were obtained from rats raised on diets containing different amounts of the element manganese. A linear plot was obtained only for the manganese-deficient sample of HDL_2. From the equation of the straight line for this sample, the Stern–Volmer constant was determined as $0.88\,M^{-1}$. The plots were non-linear for the other samples, indicating the presence of more than one class of fluorophores, which are unequally accessible to the charged I^- quencher. In Figure 13, the fluorescence quenching of HDL_1 by iodide in the presence of various amounts of the non-ionc quencher acrylamide are shown using a modified Stern–Volmer method. The plots are all linear and provide fluorescence quenching parameters characteristic of interior and surface-exposed residues. Table 1 shows a listing of the quenching constants for the different samples.

A statistical analysis of the parameters in Table 1 indicates that the acrylamide quenching constant for exposed fluorophores is significantly different in manganese-adequate HDL_1 compared with manganese-deficient HDL_1. In manganese-adequate HDL_2, there were two populations of fluorophores accessible to acrylamide, whereas in manganese-deficient HDL_2, all fluorophores were accessible to both quenchers. It was concluded based on these results that the local environments of the external fluorophores have different structures and charge distribution in manganese-adequate HDL_1 versus

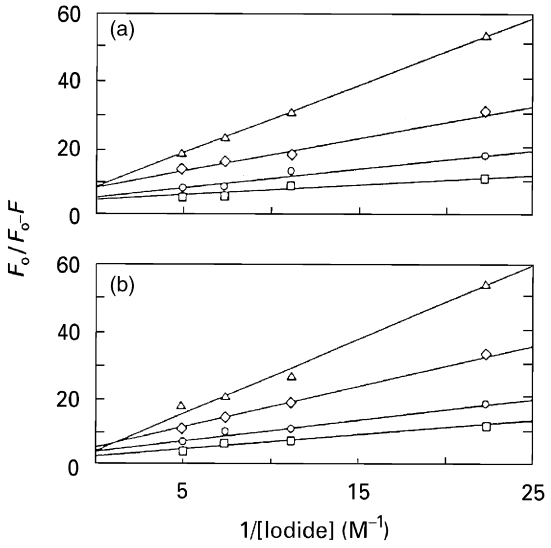

Figure 13 A modified Stern–Volmer plot for the fluorescence quenching of HDL_1 by iodide in the presence of varying amounts of acrylamide. The data are shown for HDL_1 samples obtained from rats fed with manganese-deficient (top) and manganese-adequate (bottom) diet. The fluorescence was monitored at 338 nm (I_{exc} = 295 nm) characteristic of tryptophan residues. Reproduced with permission from Taylor PN, Patterson HH, and Klimis-Tavatzis DJ (1997) A fluorescence double-quenching study of native lipoproteins in an animal model of manganese deficiency. *Biological Trace Element Research* 60: 69–80.

Table 1 Quenching constants for tryptophan residues in different high-density lipoprotein samples

Quenching constant/M^{-1}	*Lipoprotein*			
	HDL_1		HDL_2	
	MnA	MnD	MnA	MnD
K_I	9.14 ± 0.44	17.18 ± 7.72	4.63 ± 0.00	0.88 ± 0.00
K_{A1}	5.21 ± 0.88	6.15 ± 1.50	1.61 ± 0.50	–
K_{A2}	4.27 ± 0.11	5.96 ± 0.05	1.51 ± 0.00	–

MnA, manganese-adequate sample; MnD, manganese-deficient sample; K_I, iodide quenching constant; K_{A1} and K_{A2}, acrylamide quenching constant for exposed and partly exposed fluorophores, respectively.

manganese-deficient HDL_1. For HDL_2 samples, it was concluded that one-third of the fluorophores were accessible to iodide and all external and internal fluorophores were accessible to acrylamide in manganese-adequate samples, whereas in manganese-deficient samples, all fluorophores were accessible to both quenchers.

Energy Transfer

Theory

Energy transfer refers to a process in which an excited atom or molecule (*donor*) transfers its excitation energy to an *acceptor* atom or molecule during the lifetime of the donor excited state. Figure 14 shows that as a result of energy transfer, the donor returns to its ground state while the acceptor is promoted to its excited state. If the acceptor is a luminescent species, it can emit by virtue of energy transfer, that is the acceptor luminesces as a result of the excitation of the donor. Such a luminescence is called 'sensitized luminescence', and some textbooks use the terms 'sensitizer' and 'activator' instead of 'donor' and 'acceptor'. Many applications in chemistry, physics, materials science and biochemistry are based on sensitized luminescence. A later section provides an example of the application of energy transfer processes in biological systems. Energy transfer processes occur via radiative or non-radiative mechanisms.

Radiative Mechanisms

This mechanism involves the absorption of light by a donor atom or molecule (D) followed by emission of a photon by the donor and the absorption of the emitted photon by another molecule called the acceptor (A). The process can be represented as follows:

$$D + h\nu \rightarrow D^* \quad [23]$$

$$D^* \rightarrow D + h\nu' \quad [24]$$

$$A + h\nu' \rightarrow A^* \quad [25]$$

The radiative mechanism is important if the acceptor A absorbs at the wavelength at which the donor emits. The efficiency of the process is determined simply by the quantum yield of the donor luminescence and the absorbance of the acceptor at the donor emission wavelength. No significant interaction between A and D is required in this mechanism and, therefore, radiative energy transfer can occur over extremely large separations of D and A. The radiative mechanism is not important if A and D are similar molecules because of the usually small overlap of the emission and absorption spectra in this case.

Non-Radiative Mechanisms

The radiative mechanism is a trivial case of energy transfer because it can be characterized by measuring the donor absorption and the acceptor emission separately from each other. In fact, most textbooks refer to the radiative pathway as a 'trivial mechanism' for energy transfer and do not really consider it as an energy transfer mechanism. Note in Figure 14 that the donor does not emit light. Instead, the excitation energy is transferred non-radiatively to the acceptor. The non-radiative pathway shown in Figure 14 is the mechanism that is typically used in most textbooks to represent energy transfer processes. Non-radiative energy transfer processes occur via two major mechanisms, the *Förster resonance mechanism* and the *Dexter exchange mechanism.*

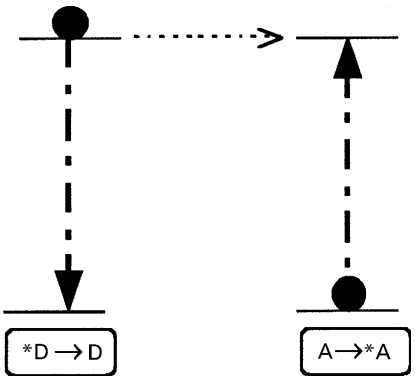

Figure 14 Energy transfer from a *donor* (D) to an *acceptor* (A).

The *Förster resonance mechanism* involves an electrostatic interaction between D and A. Such an interaction can occur over a long range, that is it does not require a very short contact between the donor and the acceptor. Energy transfer via the resonance mechanism may proceed over donor–acceptor distances as long as 50–100 Å. In order for energy transfer to be efficient via the resonance mechanism, the energies of the donor and acceptor transitions $D^* \rightarrow D$ and $A \rightarrow A^*$ must be nearly identical (hence the name '*resonance mechanism*'). Nevertheless, the presence of phonons (vibrational quanta) may provide assistance for energy transfer when small differences exist between the donor and the acceptor excited states. Such processes are called *phonon-assisted* energy transfer processes (**Figure 15**). The energies of the phonons should be high enough to surmount the difference between the donor and acceptor excited states. However, too high phonon energies increase the likelihood of non-radiative de-excitation (see above), which would take place before energy transfer can take place.

The *Dexter exchange mechanism* involves a direct contact between the donor and the acceptor atoms or molecules. The exchange interaction between the donor D and the acceptor A involves a transition state with a D–A distance that is close to the sum of the gas-kinetic collision radii of D and A, respectively. Therefore, information about the energy transfer mechanism can be gained by structural studies of the system under consideration. If the D–A distance is short (normally < 5 Å) then the exchange mechanism is the more likely, but if the D–A distance is long ($\gg 5$ Å) then the resonance mechanism would be more likely.

The energy transfer efficiency is strongly dependent on the spectral overlap between the donor emission and the acceptor absorption. This is valid for both exchange and resonance mechanisms, as shown in the following expression for the energy transfer rate:

$$k_{ET} = f(r_{D-A}) \int I_D \varepsilon_A \, d\bar{\nu} \qquad [26]$$

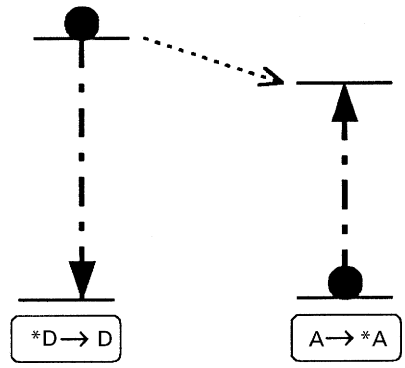

Figure 15 Phonon-assisted energy transfer. The energy difference between the excited states of D and A is provided by phonons.

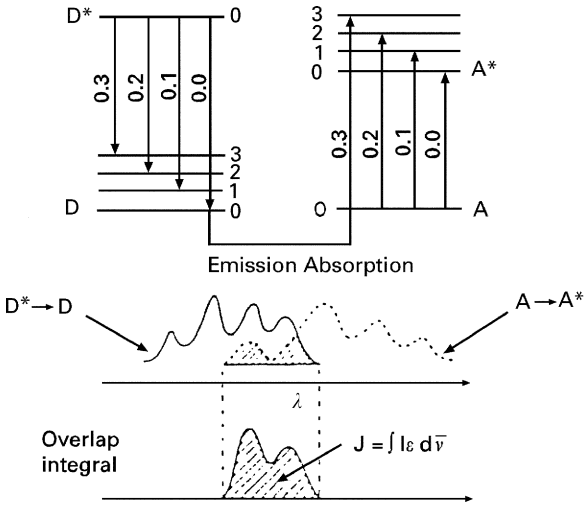

Figure 16 Experimental determination of the donor–acceptor spectral overlap from emission and absorption spectra. Reproduced with permission from Turro NJ (1978) *Modern Molecular Photochemistry*, p. 299. Menlo Park: Benjamin/Cummings.

where the integral represents the spectral overlap between the donor emission I_D and the acceptor absorption ε_A. The factor $f(r_{D-A})$ is a function of the intermolecular distance between the donor and acceptor centres (r_{D-A}) and is governed by the relevant energy transfer mechanism (Förster or Dexter mechanism). The donor–acceptor spectral overlap can be determined experimentally by spectroscopic measurements, as illustrated in **Figure 16**.

Example

Trivalent lanthanide ions, Ln(III), can be substituted for certain metal ions in proteins to gain structural information about the sites of these metals. The ability of Ln(III) ions to substitute for metal ions such as Ca(II), Zn(II), and Mn(II) in proteins stems from the similarity between Ln(III) and these ions in ionic radii, coordination

numbers (6–9) and preference to oxygen donor ligands. The higher charge density of Ln(III) makes these ions substitute with higher affinity than the metal ions in many metal-binding proteins. The quantum yield of luminescence is low for free Ln(III) but increases upon binding in close proximity to an aromatic amino acid within the protein: phenylalanine (Phe), tyrosine (Tyr) or tryptophan (Trp). When the protein is irradiated with wavelengths that correspond to the absorption maxima of these amino acids (~250–300 nm), the luminescence bands of the bound Ln(III) are enhanced by energy transfer. The strong sensitized luminescence of the Ln(III) makes these ions act as 'probes' of detailed and accurate structural information about the metal-binding sites in the proteins studied, as illustrated in the following example.

The protein α-lactalbumin is involved in the regulation of lactose synthesis. The binding of bovine α-lactalbumin (BLA) to Ca(II) is very strong ($\log K = 8$–9). Eu(III) can bind apo-BLA (apo: metal-free) in the Ca(II) binding site. The appearance of sensitized luminescence for Eu(III) is illustrated in **Figure 17**. Note that owing to energy transfer, the luminescence intensity of BLA-bound Eu(III) (upper curve) is much stronger than the intensity of free Eu(III) (lower curve). **Figure 17** shows that the increase in the intensity of the $^5D_0 \rightarrow {}^7F_2$ transition is most drastic when the ratio (R) of [Eu(III)]/[BLA] is between 1 and 2, and the intensity continues to increase when $R > 2$. This is an indication of the binding of at least two Eu(III) ions to BLA. The Eu(III) luminescence is recorded in **Figure 17** for the $^5D_0 \rightarrow {}^7F_2$ *hypersensitive* transition. A hypersensitive transition is a transition whose intensity is extremely sensitive to changes in the environment of the Ln(III) ion. Hypersensitivity is exhibited because of the $\Delta J = 2$ quadrupolar

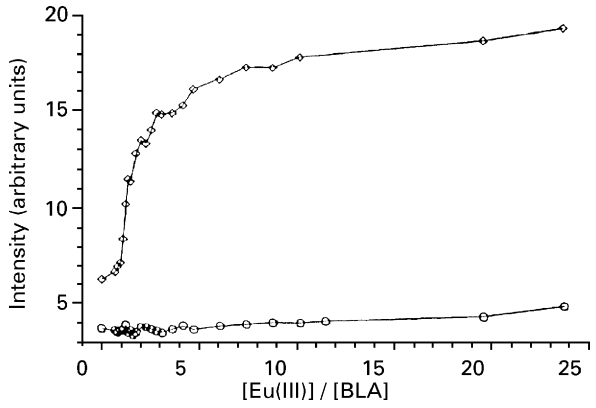

Figure 17 Luminescence titration of apo-α-lactalbumin (BLA) with europium chloride in D_2O. The luminescence intensity is monitored for the $^5D_0 \rightarrow {}^7F_2$ emission line of Eu(III) with $\lambda_{exc} = 395$ nm. The upper curve shows the data for BLA-bound Eu(III) and the lower curve shows the data for $EuCl_3$ alone. Reproduced with permission from Bünzil JCG and Choppin GR (1989) *Lanthanide Probes in Life, Chemical and Earth Sciences*, p. 279. Amsterdam: Elsevier.

nature of the transition. The importance of this transition in the BLA-bound Eu(III) is illustrated in **Figure 18**. The excitation spectra of the Eu(III)-bound BLA are shown in **Figure 18** monitoring the $^5D_0 \rightarrow {}^7F_0$ emission. The excitation spectra are resolved into several components, especially for R values >1. The appearance of bands I and II indicates the presence of two different binding sites for Eu(III) in BLA. Band III is due to non-bonded (solvated) Eu(III) ions. Therefore, it is concluded that Eu(III) ions displace Ca(II) ions from BLA and bind into two sites.

Besides the determination of the number of metal binding sites, luminescence studies of Ln(III) ions in biological systems allow the determination of other structural properties of proteins such as the number of bonded water molecules, the sum of ligand formal charges and the site symmetry of the metal ion sites. For example, lifetime measurements in H_2O/D_2O mixtures allow the determination of the number of water molecules (n) that are coordinated to the metal ions in the different binding sites:

$$n = 1.05[1/\tau(H_2O) - 1/\tau(D_2O)] \qquad [27]$$

In the preceding example, the numbers of coordinated water molecules in sites I and II were determined as 2 and 4, respectively.

Excimers and Exciplexes

Theory

Excimers and exciplexes are excited state complexes. An *excited* state di*mer* is called an *excimer*. Excimer formation can be represented by the following equation:

$$A + {}^*A \rightarrow {}^*[A - A] \qquad [28]$$

where the asterisks refer to species in their excited states. According to eqn [28], an excimer is formed when an excited molecule interacts with another identical ground state molecule. As a result of this interaction, an actual bond forms between the two monomer atoms in the excited state. Excited state interactions are not limited to the formation of homonuclear diatomic complexes. If interaction occurs between an excited molecule of one type and a ground state molecule of a different type, the resulting *excited* state com*plex* is called an *exciplex*:

$$A + {}^*B \rightarrow {}^*[A - B] \qquad [29]$$

An exciplex can also form if more than two atoms are involved in the excited-state bond, whether these atoms are identical or different. Therefore, we can write a general equation to represent exciplex formation:

$$n\,A + m^*B \rightarrow {}^*[A_n - B_m] \qquad [30]$$

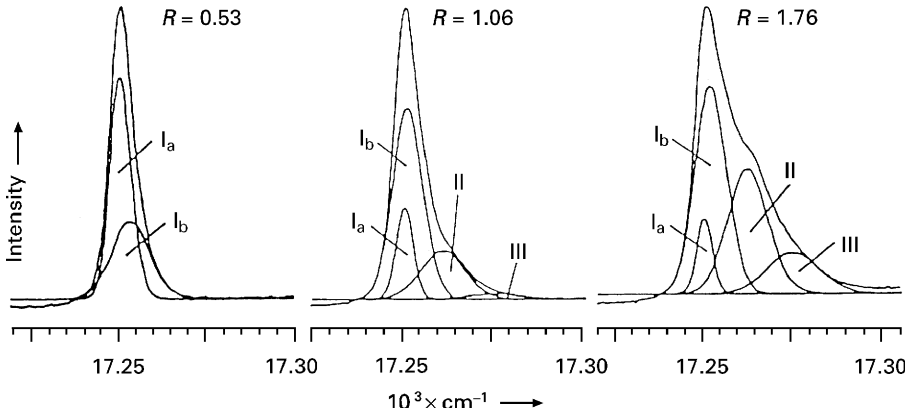

Figure 18 Curve-resolved Eu(III) excitation spectra of apo-BLA in D_2O. *R* represents the [Eu(III)]/[BLA] ratio. Reproduced with permission from Bünzil JCG and Choppin GR (1989) *Lanthanide Probes in Life, Chemical and Earth Sciences*, p. 280. Amsterdam: Elsevier.

From eqn [30], it is clear that an excimer is a special kind of exciplex where A = B and $n = m = 1$, so it is more appropriate to use the term *exciplex* when referring to excited state complexes in general, including both homoatomic and heteroatomic species.

It is important to recognize that exciplex formation is a physical phenomenon and not a chemical one. That is, bonding between the molecules only lasts as long as the excited state lifetime of the molecule, and the exciplex bond dissociates upon radiative or non-radiative de-excitation. Nevertheless, there are cases in which exciplex formation leads to photochemical reactions. For example, exciplexes are believed to be the reactive intermediates in the photochemical pathway of the Diels–Alder cycloaddition reactions of unsaturated organic compounds. Since photoluminescence is a photophysical process, the focus here will be on the photophysical aspect of exciplex formation instead of the photochemical reactions that result from exciplex formation.

Example of an Organic Exciplex

The characteristics of exciplex emission can be understood from potential energy diagrams of exciplex-forming species. **Figure 19** illustrates the spectroscopic features of exciplexes in relation to the potential surfaces of the ground and the excited electronic states. The spectra and potential surfaces are shown for pyrene, the classical example for excimer emission in organic compounds. According to **Figure 19**, the ground state is repulsive (no potential well) and the excited state is strongly bonding (deep potential well) along the pyrene–pyrene internuclear distance. This explains why the excimer bond forms only in the excited state.

Organic exciplexes are best identified by studying the variation of their emission spectra with concentration. This is illustrated in **Figure 19** for pyrene (py). At low

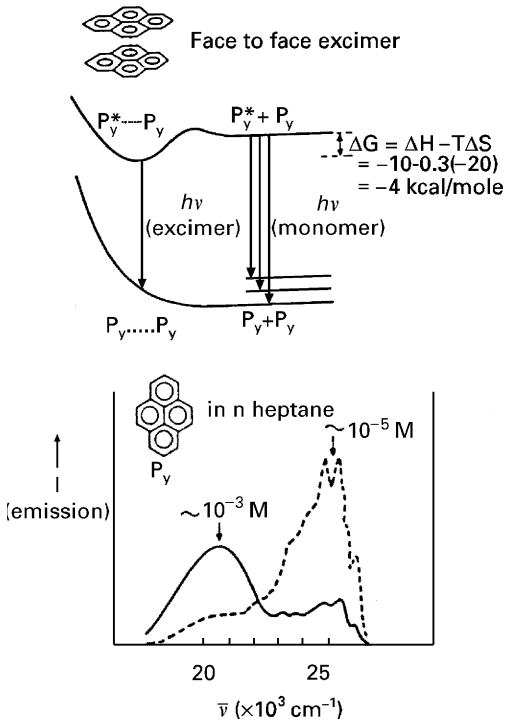

Figure 19 Excimer emission of pyrene. The upper curves show the potential surfaces of the ground and the luminescent excited electronic state. Reproduced with permission from Turro NJ (1978) *Modern Molecular Photochemistry*, p. 141. Menlo Park: Benjamin/Cummings.

pyrene concentrations ($\leq 10^{-5}$ M), the major luminescence band is due to the monomer. The characteristics of the monomer emission include: (i) vibronic structure is present, and (ii) the emission profile is independent of concentration at concentrations $\leq 10^{-5}$ M. As the pyrene concentration is increased above 10^{-5} M, the monomer emission is quenched and a new lower-energy emission band appears due to the formation of a

*[py–py] excimer. The intensity of the excimer band increases with a concentration increase. The characteristics of the excimer emission band of pyrene in Figure 19 are: (i) it is a structureless band with no vibronic structure, (ii) it has a lower energy than the monomer emission band and (iii) its intensity increases relative to the monomer emission band as the concentration is increased above a critical value (10^{-5} M for pyrene). These characteristics of the pyrene excimer bands are valid for the emission bands of organic exciplexes in general.

Examples of Inorganic Exciplexes

The formation of inorganic exciplexes has attracted attention only relatively recently. Exciplexes formed in coordination compounds could be either *ligand-centred exciplexes* or *metal-centred exciplexes*. Ligand-centred exciplexes are normally formed from coordinatively saturated complexes (where the metal ion has a high coordination number with no 'vacant' sites) and another species. In this situation, excitation of a ligand in the complex may result in the formation of an exciplex bond between the ligand and another molecule that exists in the solution (such as a solvent molecule). Metal-centred exciplexes, on the other hand, are normally formed from coordinatively unsaturated complexes and another species. In coordinatively unsaturated complexes, the potential coordination site(s) present in the metal ion can be filled by neutral electron-donor species (Lewis bases), anions or another metal ion. The latter type gives rise to the formation of *metal–metal bonded exciplexes*. This class of inorganic exciplexes is rather interesting because thus far all reported examples are luminescent.

The formation of the silver–silver bonded exciplexes $^{*}[Ag(CN)_2]_n$ ($n \geq 2$) will serve as an illustration. The formation of these exciplexes in the solid state has been reported by the authors of this article. The $[Ag(CN)_2^-]$ complex ion is a good candidate for the formation of metal–metal bonded exciplexes because its low coordination number (2) implies that several potential coordination sites are available.

Single crystals have been grown from a saturated solution of KCl that contains small amounts of $K[Ag(CN)_2]$. The crystals harvested from this solution are called $[Ag(CN)_2^-]$/KCl *doped crystals*, that is, $[Ag(CN)_2^-]$ guest ions are incorporated into (or *doped in*) the KCl host lattice. In these doped crystals, the Ag^+ and CN^- ions replace the K^+ and Cl^- ions, respectively, in some sites in the KCl lattice. Infrared measurements of single crystals of $[Ag(CN)_2^-]$/KCl have shown that multiple peaks exist in the ν_{C-N} region, indicating the presence of several local environments for the $[Ag(CN)_2]^-$ ions within the KCl lattice. This result has been explained in terms of the presence of monomers, dimers, trimers, etc. of $[Ag(CN)_2^-]$ in the doped crystal.

The luminescence spectra of $[Ag(CN)_2^-]$/KCl doped crystals at 77 K are shown in Figure 20. It is interesting to note that at least four emission bands appear in the luminescence spectra of a single crystal of $[Ag(CN)_2^-]$/KCl. The most prominent bands are labelled as A, B, C and D in Figure 20. This observation is consistent with the conclusion based on the infrared spectra that the $[Ag(CN)_2^-]$ ions exist as monomers, dimers, trimers, etc in the KCl lattice. Therefore, $[Ag(CN)_2^-]_n$ oligomer ions in the KCl lattice with different values of n are responsible for the different luminescence bands. The strong dependence of the emission spectra on the excitation wavelength is unusual because emission spectra of luminescent materials are usually independent of the excitation wavelength. By controlling the excitation wavelength, a specific $[Ag(CN)_2^-]_n$ oligomer can be excited independently from the other oligomers so that the luminescence occurs primarily from this excited oligomer. That is, different $[Ag(CN)_2^-]_n$ oligomers in

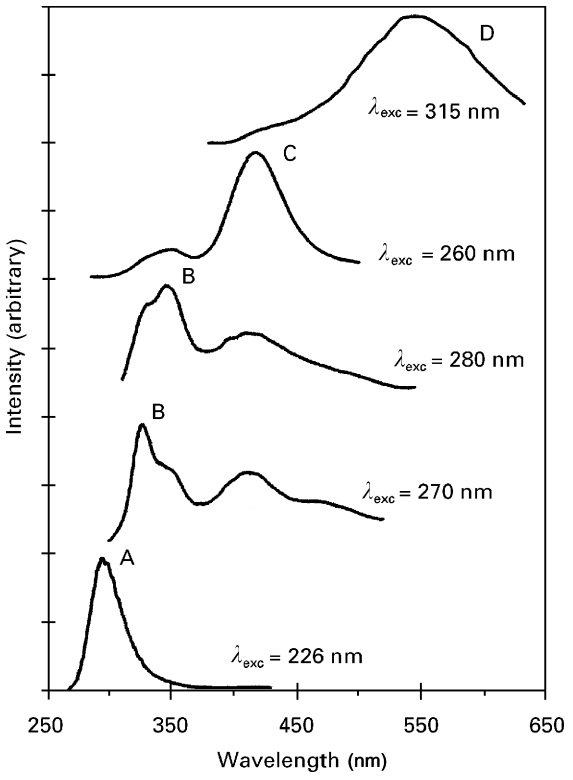

Figure 20 Photoluminescence spectra of $[Ag(CN)_2^-]$/KCl] doped crystals at 77K. The letter assignment of the luminescence bands follows the notation used in Table 2. Reproduced with permission from Omary MA and Patterson HH (1998) Luminescent homoatomic exciplexes in dicyanoargentate (I) ions doped in alkali halide crystals: 1. Exciplex tuning by site-selective excitation. *Journal of the American Chemical Society* 120: 7696–7705.

the KCl lattice act as independent luminophores, each of which has a characteristic excitation wavelength. The emission is *tuned* to any of the bands A–D by changing the excitation wavelength. This is an interesting optical phenomenon that has been called *exciplex tuning*.

The luminescence bands of $[Ag(CN)_2^-]$/KCl are assigned, as shown in **Table 2**, to $^*[Ag(CN)_2]_n$ exciplexes that differ in the value of n and in their geometry. The exciplex assignment of these bands is based on both experimental and theoretical considerations. The following is an overview of the evidence used for this assignment:

(1) The energies of the luminescence bands of $[Ag(CN)_2^-]$/KCl are extremely low relative to the absorption bands of dilute solutions of $[Ag(CN)_2]$ (which represent the $[Ag(CN)_2^-]$ monomer).

The absorption spectra of dilute solutions of $[Ag(CN)_2^-]$ show peak maxima with energies $> 50\,000\,cm^{-1}$. The excitation and emission maxima are red-shifted by as much as $23\,000$ and $30\,000\,cm^{-1}$, respectively, from the monomer transition. These large red shifts must be due to the oligomerization of $[Ag(CN)_2^-]$ units, as suggested by electronic structure calculations (see below).

The fact that the Ag(I) ion has a $4d^{10}$ closed shell electronic configuration forbids the formation of strong Ag–Ag bonds in the ground state. Excited states such as $4d^9 5s^1$, however, do not have a closed shell configuration. Hence, Ag–Ag bonding in the excited state is possible, which leads to the formation of $^*[Ag(CN)_2^-]_n$ exciplexes. **Figure 21** depicts the potential surfaces of the ground state and the first excited state of a $[Ag(CN)_2^-]_2$ dimer, as plotted from electronic structure calculations. The formation of a $^*[Ag(CN)_2^-]_2$ excimer is illustrated by the deep potential well in the excited state at a shorter Ag–Ag equilibrium distance than the corresponding ground state distance. The electronic transitions depicted in **Figure 21** explain the low emission and excitation energies (transitions (a) and (b)) relative to the monomer absorption (transition (c)).

Table 2 Assignment of the luminescence bands of $[Ag(CN)_2^-]$/KCl doped crystals

Band	λ^{em}_{mas} *nm*	λ^{exc}_{mas} *nm*	*fwhm/* $(10^3\,cm^{-1})$	*Assignment*
A	285–300	225–250	3.31	$^*[Ag(CN)_2^-]_2$ (excimers)
B	310–360	270–390	3.70	Angular $^*[Ag(CN)_2^-]_3$ (trimer exciplexes)
C	390–430	250–270	3.05	Linear $^*[Ag(CN)_2^-]_3$ (trimer exciplexes)
D	490–530	300–360	4.01	$^*[Ag(CN)_2^-]_n$ ($n \geq 5$, delocalized exciplexes)[a]

[a] It is assumed that the stabilization due to Ag–Ag interactions converges in $[Ag(CN)_2^-]_n$ oligomers with $n \geq 5$.

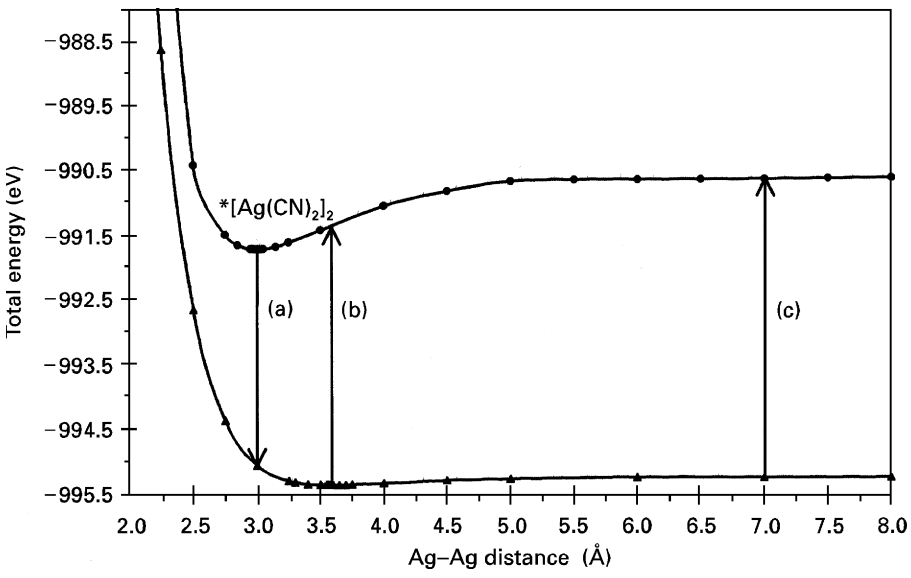

Figure 21 Potential energy diagram of the ground and the first excited electronic states of $[Ag(CN)_2^-]_2$ (eclipsed configuration) as plotted from extended Hückel calculations. The excimer $[Ag(CN)_2^-]_2$ corresponds to the potential minimum of the excited state. The optical transitions shown are (a) excimer emission, (b) solid state excitation and (c) dilute solution absorption. Reproduced with permission from Omary MA and Patterson HH (1998) Luminescent homoatomic exciplexes in dicyanoargentate (I) ions doped in alkali halide crystals: 1. Exciplex tuning by site-selective excitation. *Journal of the American Chemical Society* 120: 7696–7705.

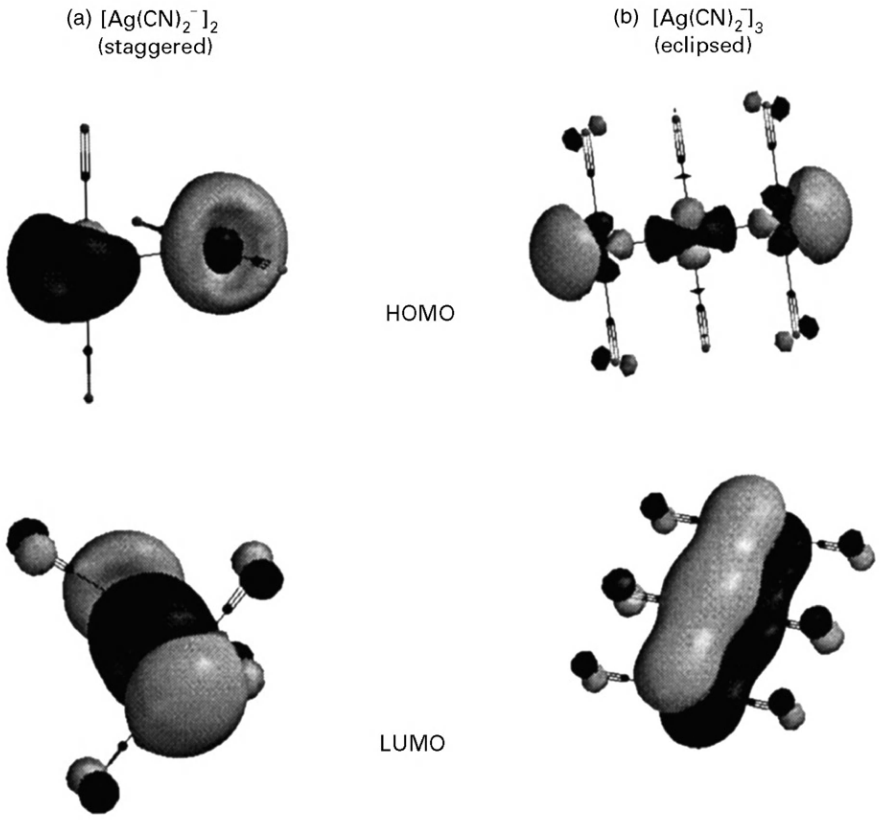

Figure 22 Surfaces of the highest occupied molecular orbital (HOMO) and the lowest unoccupied molecular orbital (LUMO) for [Ag(CN)$_2^-$]$_2$ (staggered isomer) and [Ag(CN)$_2^-$]$_3$ (eclipsed isomer), as plotted from *ab initio* calculations. Note the Ag–Ag antibonding character for the HOMO and the Ag–Ag bonding character for the LUMO in both cases.

(2) The excited states of [Ag(CN)$_2$]$_n^-$ oligomers are largely distorted from their ground states.

The Stokes shifts for the luminescence bands of [Ag(CN)$_2^-$]/KCl range from 7000 to 15 000 cm^{-1}. The fwhm values are in the 3000–4000 cm^{-1} range (**Table 2**), which are large values. As explained earlier, large excited state distortions are due to large differences in the bonding properties between the molecular orbitals that represent the ground and excited states, respectively. The ground state of an exciplex is antibonding while its first excited state is bonding. **Figure 22** illustrates this fact for the dimer [Ag(CN)$_2^-$]$_2$ and the trimer [Ag(CN)$_2^-$]$_3$. In both cases, the HOMO has a Ag–Ag antibonding character while the LUMO has a Ag–Ag bonding character. Similar results were obtained for other [Ag(CN)$_2^-$]$_n$ oligomers. Photoexcitations from antibonding HOMOs to bonding LUMOs lead to the formation of *[Ag(CN)$_2$]$_n$ exciplexes.

(3) The luminescence bands are generally lacking in structure.

Note that all the luminescence bands shown in **Figure 20** have no detailed structure. This is a similar feature to exciplex emission in organic compounds, as illustrated in **Figure 19** for the excimer band of pyrene. The apparent structure for band B is due to the existence of two different geometrical isomers of the [Ag(CN)$_2^-$]$_3$ trimer, not to vibronic structure. The absence of structured emission was obtained for [Ag(CN)$_2^-$]/KCl even though the luminescence measurements were carried out in the solid state for a doped crystal (1.1 mol% Ag) at cryogenic temperature (77 K). Doping and low temperatures normally reduce the chances of band broadening for luminophores that do not exhibit exciplex emission. Hence, the structureless emission of [Ag(CN)$_2^-$]/KCl must be due to exciplex formation.

Chemiluminescence

When exothermic chemical reactions occur, the product species are usually in their ground electronic states. However, some chemical reactions produce product species in electronically excited states which luminesce. This phenomenon is called *chemiluminescence*. Incidentally, chemiluminescence occurs in a number of biological systems (for example, the firefly), where it is called bioluminescence.

A common example of chemiluminescence is the reaction of luminol in basic solution with an oxidizing

agent such as oxygen:

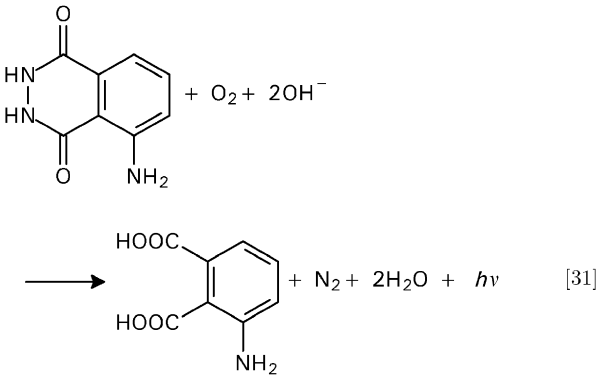

[31]

The 3-aminophthalate product ion is in an excited electronic state and shows luminescence in the visible region. Reaction [31] is catalysed by the presence of certain metal ions such as Cr(III) and the intensity of the chemiluminescence has been found to be proportional to the concentration of the specific metal ion, usually in the concentration range of parts per billion (ppb). Thus, the luminol reaction can be used to determine the concentration of selected metal ion species at very low concentrations.

A second common example of chemiluminescence in the gas phase is the reaction of nitric oxide with ozone:

$$NO + O_3 \rightarrow O_2 + NO_2^*(\rightarrow NO_2 + h\nu) \qquad [32]$$

Here, the product species NO_2 is produced in an excited electronic state and emits light in the visible–near IR region. It has been found that the intensity of the chemiluminescence is proportional to the concentration of NO in the ppm–ppb range. Thus, the reaction shown in eqn [32] can be used as the basis for the development of a chemical sensor for NO. The detection of NO is important because nitric oxide is a chief environmental pollutant, and also because NO plays an important role in human biology.

See also: Biochemical Applications of Fluorescence Spectroscopy, Laser Spectroscopy Theory.

Further Reading

Adamson AW and Fleischauer PD (1975) *Concepts of Inorganic Photochemistry*. New York: Wiley-Interscience.

Bünzil JCG and Choppin GR (1989) *Lanthanide Probes in Life, Chemical and Earth Sciences*. Amsterdam: Elsevier.

Cotton FA (1990) *Chemical Applications of Group Theory*, 2nd edn. New York: Wiley-Interscience.

Cowan DO and Drisko RL (1976) *Elements of Organic Photochemistry*. New York: Plenum.

Gilbert A and Baggot J (1991) *Essentials of Molecular Photochemistry*. Boca Raton: CRC Press.

Lakowicz JR (1983) *Principles of Fluorescence Spectroscopy*. New York: Plenum.

Omary MA and Patterson HH (1998) Luminescent homoatomic exciplexes in dicyanoargentate (l) ions doped in alkali halide-crystals: 1. Exciplex tuning by site-selective excitation. *Journal of the American Chemical Society* 120: 7696–7705.

Skoog DA, Holler FJ, and Nieman TA (1998) *Principles of Instrumental Analysis*, 5th edn. Philadelphia: Harcourt Brace.

Turro NJ (1978) *Modern Molecular Photochemistry*. Menlo Park: Benjamin/Cummings.

Wayne RP (1988) *Principles and Applications of Photochemistry*. Oxford: Oxford University Press.